1

# Metal Nanoparticle Decorated ZnO Nanostructure Based Dye-Sensitized Solar Cells

Gregory Thien Soon How<sup>1</sup>, Kandasamy Jothivenkatachalam<sup>2</sup>, Alagarsamy Pandikumar<sup>3</sup>, and Nay Ming Huang<sup>4</sup>

## 1.1 Introduction

Solar energy has always been an ideal renewable energy source that is clean, abundant, inexpensive, and widely distributed regionally in the world [1-3]. Understanding this, the emergence of dye-sensitized solar cells (DSSCs) for converting solar energy to electricity has been very promising due to the ease of the manufacturing process, the low fabrication cost, the fact that it is nonpolluting, and the relatively high efficiency [1, 4-6]. It is known that a typical DSSC consists of various subsections, including a nanocrystalline semiconductor oxide photoanode, dye sensitizer, redox couple electrolyte, and counterelectrode [3, 4]. The main idea behind the operating principle of DSSCs is based on the optical excitation of a dye that results in the injection of an electron into the conduction band of a wide band gap semiconductor oxide. The oxidized dye molecule is regenerated afterwards when it is reduced to its ground state by gaining one electron from a redox couple that is found in the electrolyte around the sensitized semiconductor oxide nanostructured film [3-5]. Since the first outstanding research work on DSSC was demonstrated by O'Regan and Gratzel in 1991 [5], each of its components has been extensively investigated and optimized, with the aim to maximize the power conversion efficiency (PCE) of DSSCs [4, 7, 8]. Recently, a PCE of 12.3% has been achieved by using the cosensitization of two dyes

<sup>&</sup>lt;sup>1</sup> Department of Physics, University of Malaya, Malaysia

<sup>&</sup>lt;sup>2</sup> Department of Chemistry, Anna University-BIT Campus, Tiruchirappalli-620024, Tamilnadu, India

<sup>&</sup>lt;sup>3</sup> Functional Materials Division, CSIR-Central Electrochemical Research Institute, Karaikudi-630006, India

<sup>&</sup>lt;sup>4</sup> Faculty of Engineering, University Xiamen Malaysia, Malaysia

and a Co(II/III) tris(bipyridyl)-based redox electrolyte [9]. Hence, study to find a suitable and high performance DSSC output has greatly increased over the years.

Amongst all the materials studied for use in DSSCs, nanocrystalline  ${\rm TiO_2}$  has been most commonly employed as the metal oxide semiconductor material in high efficiency DSSCs [4–6]. Several methods were used for the preparation of the  ${\rm TiO_2}$  nanoparticles in DSSCs, such as sol-gel [10, 11], gas-phase pyrolysis [12], or the commonly used hydrothermal synthesis method [13, 14]. However, hydrothermal methods are not ideal because both synthesis and purification processes take a prolonged time to achieve well-formed and highly crystalline  ${\rm TiO_2}$  particles [12]. To minimize the costs of metal oxide semiconductor materials for DSSCs, simple preparation methods are essential to control the formation of crystal structure, crystallization, and particle size [15]. Besides  ${\rm TiO_2}$ , there are reports of other alternative metal oxides, such as  ${\rm SnO_2}$ ,  ${\rm Nb_2O_5}$ , and  ${\rm ZnO}$ , being used as porous semiconductor materials for DSSC photoelectrodes [16–20].

ZnO is an another attractive and alternative photoanode to replace TiO<sub>2</sub> as an electron conductor owing to its higher bulk electron mobility and easily tunable morphology, which allows the rational design and development of hierarchical ZnO nanostructures able to simultaneously optimize charge carrier path and dye loading [19, 20]. Hence, ZnO is considered an excellent backbone to produce high-efficiency DSSCs. The ZnO characteristic of higher electron mobility ( $\sim 205-1000 \,\mathrm{cm}^2 \,\mathrm{V}^{-1} \,\mathrm{s}^{-1}$ ) than  $\mathrm{TiO}_2$  ( $\sim 0.1-4 \,\mathrm{cm}^2 \,\mathrm{V}^{-1} \,\mathrm{s}^{-1}$ ), enables the rapid diffusion transport of photoinjected electrons when it is employed as a photoanode material in DSSCs. In addition, ZnO is a suitable material for the fabrication of mesoporous photoanodes in DSSCs; it has a band gap of 3.2 eV and a conduction band edge position of -4.3 eV, both of which are similar to TiO<sub>2</sub> [15–17]. Moreover, ZnO can be easily prepared into tunable nanostructures, such as nanoparticles, nanowires, nanotubes, nanorods, nanosheets, and tetrapods, providing numerous alternatives for optimizing photoanode morphology so as to improve the charge collection. However, the conversion efficiency of ZnO-based DSSCs reported so far still remains lower than those fabricated from TiO2, leaving plenty of room to improve the efficiency through structural and morphology modifications of the ZnO nanostructures. Previous review articles [16, 17] have explored recent developments in ZnO nanostructures for application in DSSCs and suggest that the nanostructured ZnO can significantly enhance solar cell performance due to the large surface area for dye adsorption, direct transport pathways for photoexcited electrons, and efficient scattering centers for enhanced light-harvesting efficiency. Furthermore, the limitations of ZnO-based DSSCs are also discussed and a few suggestions are also given for the conversion efficiency improvement.

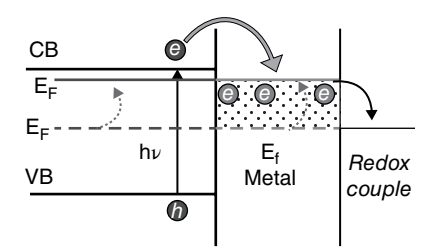
## 1.2 Metal Dressed ZnO Nanostructures as Photoanodes

One of the major challenges in the development of high efficiency DSSCs is the competition between the generation and recombination of photoexcited carriers. The use of low-dimensional nanostructures is able to support a direct pathway for the rapid collection of photogenerated electrons and, hence, reduce the charge recombination [21, 22]. Thus, the possible alternative way to improve the charge separation in DSSCs is to introduce a barrier layer at the semiconductor/electrolyte interface to block the back electron transfer from the semiconductor to the redox electrolyte. Doping of metals on ZnO nanostructures significantly reduces the charge recombination, which is another way to improve the charge separation in DSSCs. Rapid charge transfer and improved charge separation upon incorporation of metal nanoparticles on ZnO, leading to enhanced DSSC performance, have been demonstrated [23-33]. Moreover, the metal nanoparticles (namely silver and gold) that possess surface plasmon resonance can couple to visible light, which increases the optical absorption of the photoelectrode in the visible region.

Metal nanoparticles doped on ZnO exhibit unusual redox activity by readily accepting electrons either from a dye molecule or an electrode. Such metal nanoparticles, when in contact with a ZnO nanostructure, can equilibrate and undergo Fermi-level equilibration, thus forming a Schottky barrier at the metal/ZnO nanocomposite interfaces (Figure 1.1) [22].

The charge equilibration between the metal and ZnO nanocomposite interfaces in contact drives the Fermi level close to the conduction band edge of the semiconductor and, thus, influences the photovoltaic performance of DSSCs. So far, ZnO-based DSSC performance has been reviewed but there is no summary of the metal dressed ZnO based DSSC performance. In this review, the recent progress on metal dressed ZnO based DSSC and the role of metal nanoparticles on various ZnO nanostructures in DSSCs (Figure 1.2) in improving the device performance (through improved charge separation introduced by the Schottky barrier formed at the metal/ZnO nanocomposite interface) are

**Figure 1.1** Schematic representation of photoinduced charge separation and charge distribution in ZnO/metal nanocomposites. E<sub>F</sub> and E'<sub>F</sub> represent Fermi levels attained before and after charge distribution. *Source:* Adapted from Subramanian 2003 [22]. Reprinted with permission of American Chemical Society.



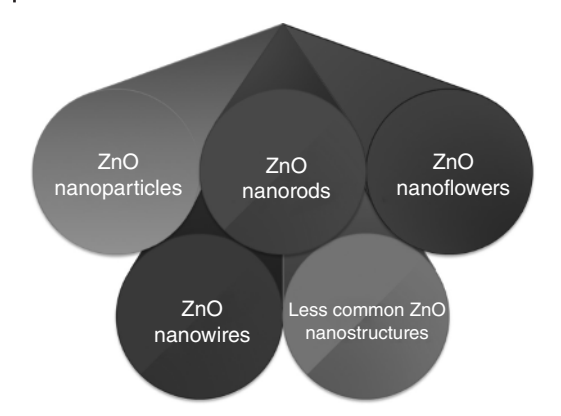


**Figure 1.2** Various types of metal dressed ZnO nanostructure used as photoanodes in DSSCs.

discussed. Furthermore, the influence of silver and gold nanoparticles leading to enhanced optical absorption on the performance of DSSCs is also discussed.

## 1.2.1 Metal Dressed ZnO Nanoparticles as Photoanodes

There are few related works reported involving metal dressed ZnO nanoparticles as photoanodes in DSSC applications. Among them, Tripathi [23] and coworkers reported a bilayer TiO<sub>2</sub>:Ag/ZnO:Ag (TZO:Ag) oxide film using a sol-gel process for DSSCs. They have investigated the effect of Eosin-Y dye and a cocktail dye (C) (Rhodamine B, Rose Bengal, Fast Green, Acridine Orange, Fast Green) for DSSC application. In comparison to the undoped ZnO/C film, their TZO/Ag/C film exhibits higher Voc, Jsc, and PCE of 0.158%. This is due to the surface plasmon resonance effect of the silver nanoparticles in enhancing visible light absorption and also the Schottky barrier established at the semiconductor/metal interface. Sarkar et al. reported a nanocomposite consisting of gold and ZnO nanoparticles (NPs) for photocatalysis and DSSC applications [24]. Their ZnO-Au nanocomposite (NC) was synthesized based on the formation of gold NPs on the surface of ZnO NPs, using chloroauric acid ethanolic solution added into readily prepared ZnO NP colloid solution. To obtain the gold NPs, they added sodium borohydride (through a chemical reduction method) in order for gold chloride to undergo reduction. Interestingly, the ZnO-Au NC morphology (Figure 1.3) reveals the uniform distribution of gold on spherical ZnO nanoparticles, with average diameters of 6nm and 8nm, respectively. In their DSSC application, the ZnO-Au NC depicts a higher overall PCE of 0.8% than the pure ZnO (PCE = 0.012%). Such major difference in the PCE reported was claimed to be attributed to role of gold in increasing the electron mobility in ZnO-Au NC in addition to its plasmon resonance.

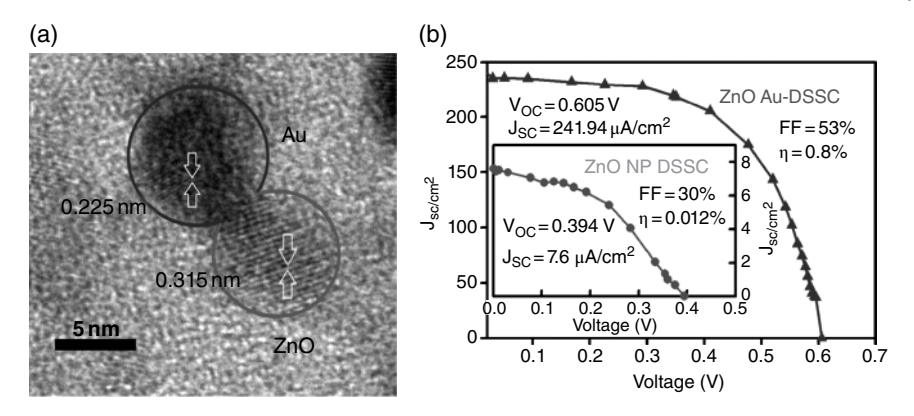


**Figure 1.3** (a) TEM image of Au@ZnO nanoparticles and (b) *I–V* curves obtained for the modified photoanode-based DSSCs using N719 dye-sensitized Au@ZnO nanoparticles. Inset: *I–V* curves obtained for the N719 dye-sensitized ZnO nanoparticles based DSSCs. Adapted from [24] with permission of The Royal Society of Chemistry.

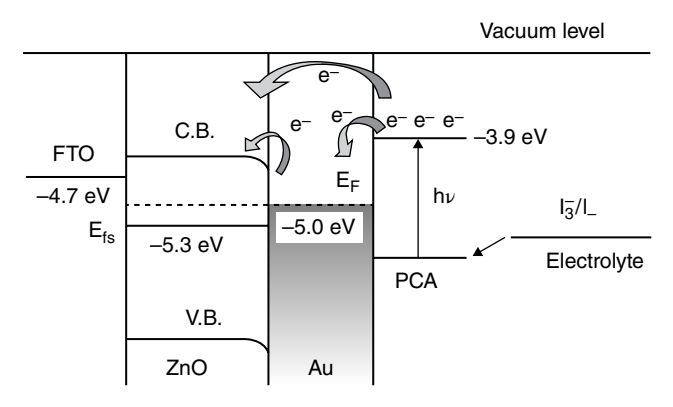


**Figure 1.4** Energy level diagram and mechanism of photocurrent generation in the DSSC with FTO/ZnO/Au/PCA/polymer electrolyte. Adapted from [25] with permission of The Royal Society of Chemistry

Mikroyannidis and coworkers also reported gold-coated ZnO photoanodes for DSSC application using their own synthesized perylene monoimide derivative, PCA, as the sensitizer (Figure 1.4) [25]. Initially, they synthesized pure ZnO NPs using a sol-gel method and then immerse the preformed ZnO NPs in chloroauric acid to obtain ZnO NPs coated with gold nanoparticles. Later, the photoanodes were immersed in their own prepared PCA sensitizer, which is a metal-free dye. By comparing their DSSC obtained PCE, it was found that the PCE of their ZnO NPs coated with gold NPs was enhanced from 1.34 to 1.91%, which contributed to the fast transport of electrons from the gold NPs to the ZnO NPS through the Fermi-level equilibration and the

formation of a Schottky barrier at the ZnO/Au interface, which reduces the charge recombination rate, thus increasing the PCE as described earlier. The PCE was also improved by adding  ${\rm TiO_2}$  nanofillers into the ZnO–Au DSSC, which again increased the PCE values to 2.44%. It was reported that the increasing PCE value in the presence of nanofillers ( ${\rm TiO_2}$ ) is due to the enhancement of exchange charge density and diffusion coefficient of triiodide, which depress the concentration of  ${\rm I_3}^-$ , and the suppression of the dark reaction by the polymer gel electrolyte with  ${\rm TiO_2}$ . The improved PCE could be due to the incorporation ZnO into  ${\rm TiO_2}$  DSSCs as a result of the inhibition of the injected electrons from the dye molecules in recombining back with the electrolyte species [34].

#### 1.2.2 Metal Dressed ZnO Nanorods as Photoanodes

Recently, great interest was shown in a ZnO nanorod (NR) structure (compared to other ZnO morphologies) due to its high surface area and its capability of rapid charge collection that enhances the overall short circuit current [35, 36]. Yin and coworkers [26] have reported on their ZnO nanorods array deposited with silver nanoparticles (Ag NPs/ZnO NRs) for DSSC application. This composite was synthesized through a combination of liquid phase epitaxial growth process and the reduction of silver on the surface of the ZnO NRs (Figure 1.5). According to this report, the role of silver NPs was seen to improve the DSSC efficiency (PCE = 0.81%) compared to the pure ZnO NRs; this can be related to the surface plasmon resonance of the silver NPs and the Schottky barrier at the Ag/ZnO interface.

Instead of using silver nanoparticles, a number of works related to dressing the ZnO nanorods with gold nanostructures have also appeared. Lou et al. reported the fabrication of gold NPs on hydrothermally prepared ZnO NR films using an ion sputtering technique [27]. Their work was mainly concerned with the effect of molecular modification on plasmon-enchanced DSSCs using the dodecanethiol molecule to protect the gold NPs from the electrolyte. The ZnO/Au/N719/dodecanethiol device recorded the highest IPCE in the range of 440-470 nm, which can be attributed to the "shielding" effect of the dodecanethiol molecules on the exposed gold nanoparticle sites that reduces the charge recombination rate. Similarly, Chen et al. reported the fabrication of a DSSC using vertically aligned ZnO nanorod arrays sensitized with gold nanoparticles [28]. Based on a low-temperature chemical seeding method, their composite was examined and compared with pure ZnO nanorod arrays, and also with and without the presence of ruthenium dye N719. Obviously, the composite photoanode in the presence of ruthenium dye exhibits the highest power conversion efficiency of 1.2%. They have claimed that the back electron transfer was significantly reduced by the interfacial ZnO-Au Schottky barrier that results in the increased efficiency.

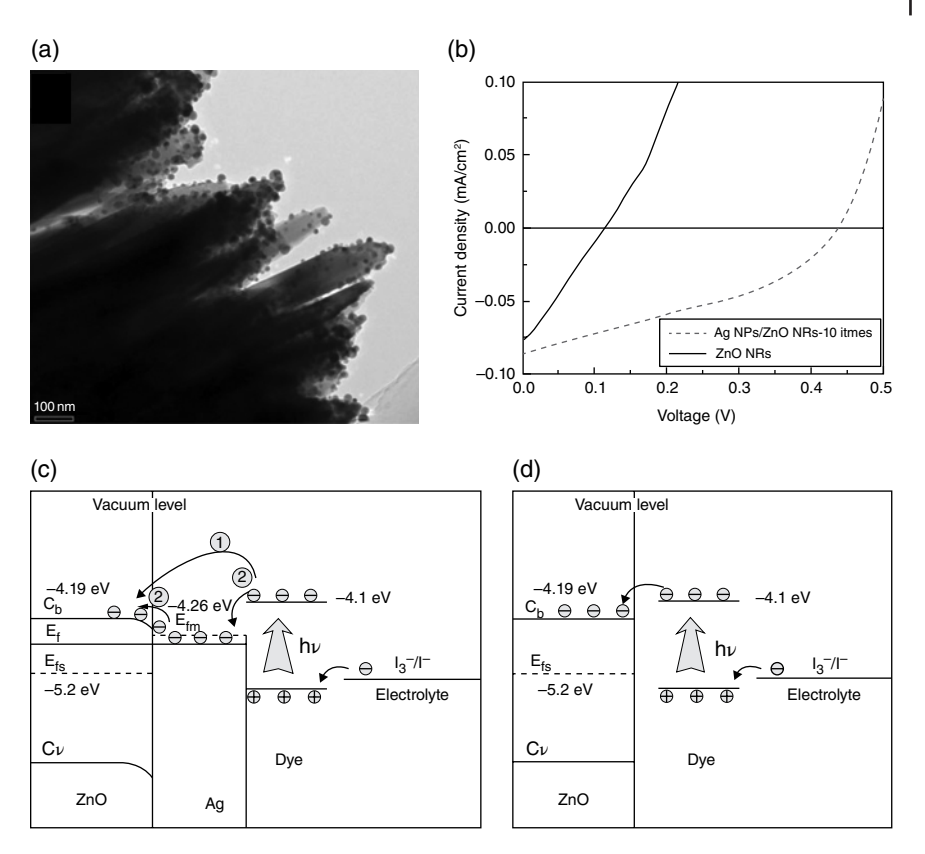


**Figure 1.5** (a) TEM image of the Ag NPs/ZnO NRs composite arrays prepared by 10 adsorption–reduction cycles and (b) *J–V* characteristics of the solar cells prepared with the bare ZnO NR arrays and the Ag NPs/ZnO NR composite arrays (free dye). Energy level diagram and mechanism of the photocurrent generation in the photoelectrochemical cell prepared with (c) the Ag NPs/ZnO NR composite arrays and (d) the bare ZnO NRs array. Reprinted by permission from Springer Nature Copyright 2012 [26].

Although the surface plasmon resonance effect is known to significantly enhance the DSSC efficiency, Peh and coworkers reported that the addition of gold nanoparticles on their ZnO nanorods has substantially reduced the overall conversion efficiency [29]. The decrease of conversion efficiency of the pure ZnO nanorod device from 5.2 to 2.5% for the Au–ZnO device is attributed to the aggregation of the gold nanoparticles that distorts the plasmonic effect, thus broadening the spectral enhancement of the device. In addition, this also decreases the surface area of ZnO nanorods adhering to the dye molecules, which dramatically reduces the sunlight conversion process. In terms of the effect of the DSSC's active area, Bora *et al.* reported the presence of a highly efficient ZnO/Au Schottky barrier in their ZnO/Au nanocomposite DSSC

[30]. They studied the effects of various sizes of the active area in the DSSC, and also the amounts of gold nanoparticles incorporated in their ZnO nanorod photoelectrodes. Their results are in good agreement with the previous work as an approximately60% decrease in PCE was reported when the amount of gold nanoparticles increased by varying the dipping time of the ZnO nanorod photoelectrodes in HAuCl<sub>4</sub>·H<sub>2</sub>O solution (0.01 mM). Furthermore, the impact of DSSC active area size was also reported, as increment in the size of the DSSC active area reveals higher sheet resistance of the used substrates. Therefore, the PCE values decrease as the active area of the DSSC increases. Through this reported work, the importance of optimizing the amount of metal nanoparticles to avoid excess aggregation occurring on the semiconductor layer, in order to fully harness the enhanced plasmonic effect of the DSSCs, is well understood, as is the size of the active area of DSSC to reduce the series resistance occurring on the substrates.

#### 1.2.3 Metal Dressed ZnO Nanoflowers as Photoanodes

ZnO nanoflowers have been of considerable interest to some researchers due to their unique structure. Through the application of the ZnO nanoflowers, it is possible to benefit from the increased dye loading and light harvesting capability whilst still maintaining satisfactory electron conductivity in the DSSC [37, 38]. Although they are plenty of works involving ZnO nanoflowers for DSSCs, there is only one known work reporting on metal dressed ZnO nanoflowers used as a photoanode. This work, by Dhas and co-workers [31] involves the loading of ZnO nanoflowers on gold nanoparticles through a simple hydrothermal route. Initially, this one-step method involves the dissolution of zinc acetate, in which the morphology is controlled later by the addition of NaOH, and then loading of gold NPs using HAuCl<sub>4</sub>. The wurzite structures of ZnO rod-like petal structures were embedded with gold NPs that are uniformly distributed with an average size of approximately 10 nm, as shown in Figure 1.6. In terms of their DSSC performance, the role of gold nanoparticles on the ZnO nanoflowers was compared with the pure ZnO nanoflower device. As expected, their *I–V* curves reveal that the bifunctional gold NP-loaded ZnO nanoflower shows enhanced properties (fill factor (FF) 0.33 and efficiency 2.5%) over the pure ZnO nanoflower device (FF 0.32 and efficiency 1.6%). Such an increase was attributed to the gold nanoparticles reducing the recombination spots due to the oxygen vacancies in ZnO in the surface layers and the surface plasmon resonance effect.

#### 1.2.4 Metal Dressed ZnO Nanowires as Photoanodes

Similar to ZnO nanorods, one-dimensional ZnO nanowires also exhibits good photoconversion enhancement, which benefits from direct conduction paths for electrons to transport from the point of injection to the collection

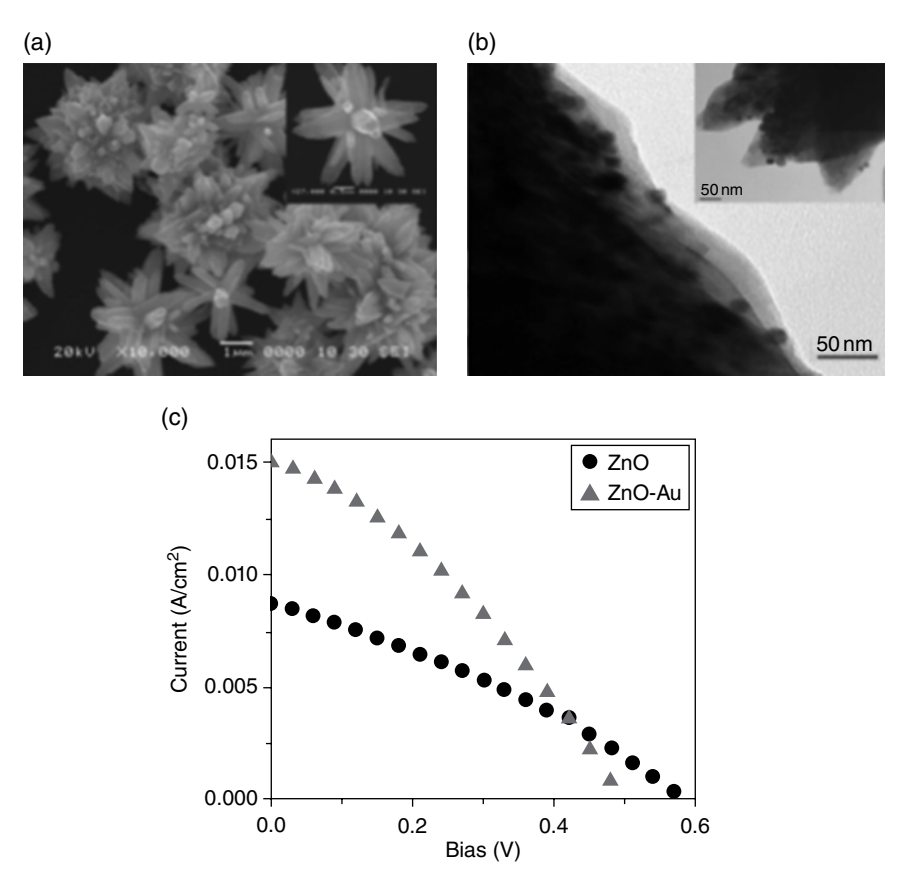


**Figure 1.6** (a) SEM image of ZnO nanoflowers with gold nanoparticles and (b) HRTEM image of ZnO nanoflower petal surface loaded with gold nanoparticles. Inset (a) a single ZnO nanoflower with gold nanoparticles and (b) gold nanoparticles loaded ZnO nanoflower petals. (c) J-V curve obtained for  $N_3$  dye-sensitized ZnO nanoflowers films with and without gold nanoparticles. Reprinted from [31] with the permission of AlP Publishing.

electrode, making them a much more preferable nanostructure in DSSC application [39, 40.] So far, they have only been reported once, by Lu and coworkers, in literature on metal dressed ZnO nanowires used in DSSC applications [32]. In their project, the synthesis was reported of vertically grown gold NPs on ZnO nanowire arrays (Au NPs @ZnO nanowire) through a two-step method. Their structure reveals that the size of the gold nanoparticles ranges from 5 to 10 nm and the shell is around 15 nm. Under solar simulation, bare ZnO nanowire arrays and the Au NPs @ZnO nanowires have been compared, with the latter displaying increased PCE values from 0.154 to 0.191% and from 0.269 to 0.387% using different length ZnO nanowire arrays (3 and 7.5  $\mu$ m, respectively). Through this research, they have concluded that a plasmonic-enhanced DSSC

requires a lower thickness (about 20-40%) to achieve the same efficiency as conventional DSSCs. However, more experimental investigation is still needed in order to verify their conclusion.

## 1.2.5 Less Common Metal Dressed ZnO Nanostructures as Photoanodes

Although the most commonly reported ZnO nanostructures, such as nanorods and nanoparticles, are widely used in plasmonic-enhanced DSSCs, less common and unique ZnO nanostructures have also been reported during investigations into the use of other alternative rare nanostructures for enhancing DSSC properties. A sheaf-like-ZnO@Ag nanocomposite (sheaf-like-(ZnO@ Ag)<sub>NCM</sub>) has been reported as the photoanode in a DSSC application [33]. The synthesis of sheaf-like-(ZnO@Ag)<sub>NCM</sub> was made through a two-step method whereby ZnO NRs were synthesized using a microwave irradiation method at 150 W. Following this, the preformed ZnO NRs were mixed with AgNO<sub>3</sub> before undergoing a reduction process with NaOH to form the sheaf-like-(ZnO@ Ag)<sub>NCM</sub>, as shown in Figure 1.7a. The morphological structure obtained (Figure 1.7b) - the sheaf-like-(ZnO@Ag)<sub>NCM</sub> - was composed entirely of 1D closely-packed nanorods with a typical diameter of about 150-200 nm. It was well understood that the unique sheaf-like structure formation takes place during the conversion of Ag<sup>+</sup> to Ag NPs with NaOH as the reducing agent.

In terms of DSSC use, the *sheaf-like-*(ZnO@Ag)<sub>NCM</sub> was pasted on fluorinedoped tin oxide (ITO) through a doctor blade method and was dipped in two different sensitizers: eosin-Y and N719 dye. The J-V graph (Figure 1.7c) shows various photoanodes used to compare the different sensitizers and sheaf-like-(ZnO@Ag)<sub>NCM</sub> with pure ZnO photoanodes. Obviously, the ZnO NR-Ag photoanodes outperformed the pure ZnO NR photoanodes; this was attributed to the effective charge separation and charge transfer and the formation of a Schottky barrier due to the introduction silver nanoparticles on ZnO. As for the different sensitizers, ZnO NR-Ag/N719 exhibits a better PCE value (1.80%) than ZnO NR-Ag/EY (1.39%). Based on this work, the N719 dye remains a more appropriate sensitizer than the eosin-Y dye, as it has a broader absorption range in the entire visible region of the solar spectrum and the presence of silver NPs.

## 1.2.6 Comparison of the Performance of Metal Dressed ZnO Nanostructures in DSSCs

The performances of the various metal dressed ZnO nanostructures described in DSSCs are listed in Table 1.1. From this table, it can be seen that most of the ZnO nanostructure DSSCs incorporating plasmonic nanoparticles have yet to achieve a high benchmark in terms of PCE values. A wide range of study is still

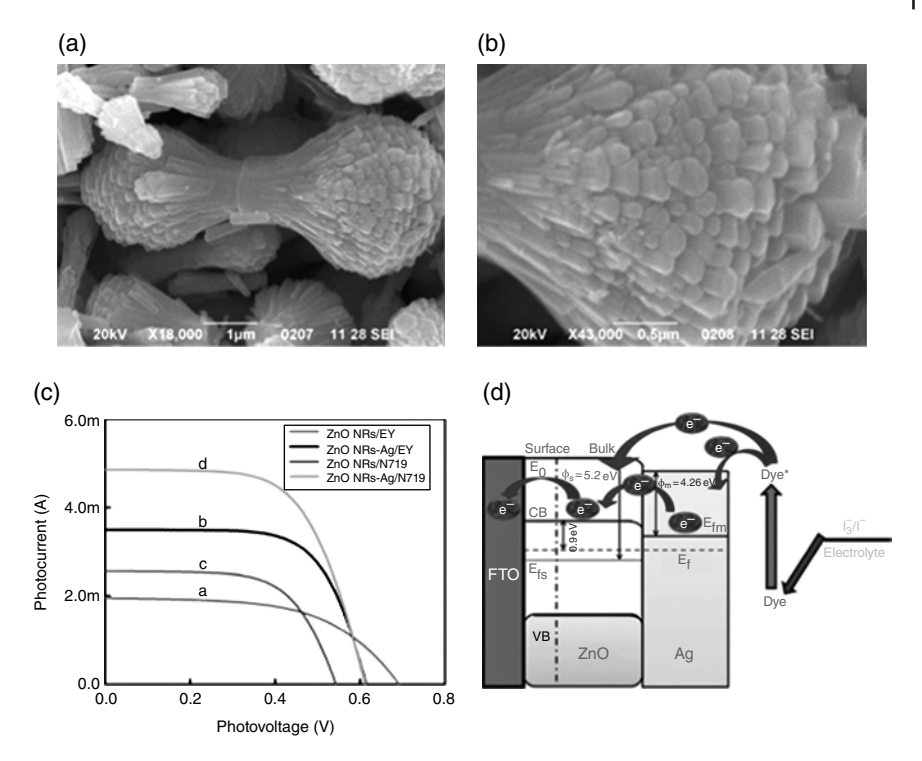


Figure 1.7 (a) and (b) SEM image of sheaf-like-(ZnO@Ag)<sub>NCM</sub>. (c) J-V curves recorded for ZnO NRs/eosin-Y, sheaf-like-(ZnO@Ag)<sub>NCM</sub>/eosin-Y, ZnO NRs/N719, and sheaf-like (ZnO@Ag)<sub>NCM</sub>/N719 photoanodes with TiO<sub>2</sub> NPs modified PEO electrolyte based solid-state DSSCs under simulated AM 1.5 G solar irradiation of 100 mW/cm². Area of the cell was 1 cm². (d) Mechanism of photocurrent generation at sheaf-like-(ZnO@Ag)<sub>NCM</sub> modified photoelectrode based dye-sensitized solar cells. Where E<sub>fs</sub> and E<sub>fm</sub> are Fermi level of semiconductor and metal, respectively.  $φ_s$  and  $φ_m$  are work function of semiconductor and metal, respectively. Reprinted from [33] with the permission of AIP Publishing.

needed to enhance DSSCs performance for it to compete against recently reported photovoltaic cells. Among the reported DSSCs, the DSSC with ZnO/Au/N719/ dodecanethiol configuration showed an efficiency of 13.5 % due to the presence of gold nanoparticles, which enhanced the interfacial charge transfer process [27].

## 1.3 Conclusions and Outlook

This chapter has explained the use of plasmonic nanoparticle dressed ZnO nanostructures involving various structural designs (nanoparticles, nanorods, nanoflowers, nanowires, less common ZnO structures) used in DSSCs. As

 Table 1.1 Comparison of various metal nanoparticle dressed ZnO nanostructure DSSCs.

Ref.

[23]

[24]

[25]

[26]

[27]

[28]

Photoanode	Fabrication method	Sensitizer	Short-circuit photocurrent Open-circuit density, J <sub>sc</sub> (mA/cm <sub>2</sub> ) voltage, V <sub>oc</sub> (V	Open-circuit voltage, V <sub>oc</sub> (V)	Fill factor, FF	Fill factor, Power conversion FF Efficiency, ղ (%)
TZO/Ag/C	Sol-gel	Eosin-Y, Cocktail Dye	0.621	0.477	53	0.158
ZnO-Au NC	Chemical reduction	N719	0.26187	0.605	53	8.0
$ZnO-Au+TiO_2$ nanofiller	Chemical reduction	PCA	6.35	0.70	55	2.44
Ag NPs/ZnO NRs	Chemical reduction	N719	I	0.44	I	0.81
Zno/Au/N719/ dodecanethiol	Ion sputtering	N719	I	I	I	13.5*
Au/ZnO NR	Chemical reduction	N719	4.2	0.62	I	1.2
Au-ZnO	Mixing	N719	1.8	0.55	63.4	2.5
ZnO/Au nanocomposite	<i>In situ</i> precipitation	N719	14.89	29.0	90:59	6.49
ZnO-Au	Hydrothermal	N3	15.00	0.50	33	2.5
Au NPs @ZnO nanowire	I	I	I	I	I	0.191
$sheaf$ - $like$ - $(ZnO@Ag)_{NCM}$ Chemical reduction	Chemical reduction	Eosin-Y, N719	4.85	0.61	61	1.80
*η (%) based on IPCE measurements	rements					

[30]

[31][32] [33]

[29]

<sup>\*</sup>η (%) base

reported, the role of the plasmonic nanoparticles was clearly observed enhancing the electrical properties of the photoanodes when attached to the ZnO nanostructures. Without a doubt, ZnO nanorods do possess a significant advantage over the other ZnO nanostructures when incorporated with plasmonic nanoparticles, as the structure itself promotes a more direct pathway for electron movement. Nonetheless, it also necessary to take into account other parameters, such as the size of the active area of the photoanode, the amount of plasmonic nanoparticles injected, and the type of sensitizer used, which could ultimately affect the final results of the DSSCs' efficiency.

Although some of the work has shown promising results for possible commercialization and applicability, these photoanodes still yield low PCE values when compared to TiO<sub>2</sub>-based photoanodes. In order to achieve higher PCE values, other alternative materials are still to be explored, such as the incorporation of plasmonic nanoparticles on a mixture of various ZnO nanostructures (nanopellets, nanosheets, nanotubes, nanofibres). Only a few works on DSSCs based on plasmonic nanoparticles on ZnO nanostructures have been reported. Much work is still needed to be done and investigated, especially with different parameters, in order for it to be on par with recent DSSCs that have reported high performance and good stability.

## References

- 1 R. Pike and P. Earis, Energy Environ. Sci., 2010, 3, 173.
- 2 P.V. Kamat, J. Phys. Chem. C, 2007, 111, 2834–2860.
- **3** L.M. Gonçalves, V. de Zea Bermudez, H.A. Ribeiro, and A.M. Mendes, *Energy Environ. Sci.*, 2008, **1**, 655.
- 4 A. Hagfeldt, G. Boschloo, L. Sun, et al., Chem. Rev., 2010, 110, 6595-6663.
- 5 B. O'Regan and M. Grätzel, *Nature*, 1991, 353, 737–740.
- 6 C.J. Barbé, F. Arendse, P. Comte, et al., J. Am. Ceram. Soc., 1997, 80, 3157–3171.
- 7 J. Cong, X. Yang, L. Kloo, and L. Sun, Energy Environ. Sci., 2012, 5, 9180.
- 8 N. Tétreault and M. Grätzel, Energy Environ. Sci., 2012, 5, 8506.
- 9 A. Yella, H.-W. Lee, H.N. Tsao, et al., Science, 2011, 334, 629-634.
- 10 D. Chen, F. Huang, Y.-B. Cheng, and R. A. Caruso, *Adv. Mater.*, 2009, **21**, 2206–2210.
- 11 M. Hočevar, U. Opara Krašovec, M. Berginc, *et al.*, *J. Sol-Gel Sci. Technol.*, 2008, **48**, 156–162.
- 12 X. Chen and S.S. Mao, Chem. Rev., 2007, 107, 2891–2959.
- 13 S. Lee, I.S. Cho, J.H. Lee, et al., Chem. Mater., 2010, 22, 1958–1965.
- 14 H. Zhang, Y. Han, X. Liu, et al., Chem. Commun., 2010, 46, 8395–8397.
- **15** Y.M. Evtushenko, S.V Romashkin, and V.V Davydov, *Theor. Found. Chem. Eng.*, 2011, **45**, 731–738.

- **16** K. Sayama, H. Sugihara, and H. Arakawa, *Chem. Mater.*, 1998, **100**, 3825–3832.
- 17 Y. Fukai, Y. Kondo, S. Mori, and E. Suzuki, *Electrochem. Commun.*, 2007, **9**, 1439–1443.
- **18** Q. Zhang and G. Cao, *Nano Today*, 2011, **6**, 91–109.
- 19 Q. Zhang, C.S. Dandeneau, X. Zhou, and G. Cao, *Adv. Mater.*, 2009, **21**, 4087–4108.
- 20 J. Anta, E. Guillén, and R. Tena-Zaera, J. Phys. Chem. C, 2012, 116, 11413–11425.
- 21 C. Xu, J. Wu, U.V. Desai, and D. Gao, J. Am. Chem. Soc., 2011, 133, 8122-8125.
- **22** V. Subramanian, E.E. Wolf, and P.V Kamat, *J. Phys. Chem. B*, 2003, **107**, 7479–7485.
- 23 S.K. Tripathi, M. Rani, and N. Singh, *Electrochim. Acta*, 2015, **167**, 179–186.
- 24 S. Sarkar, A. Makhal, T. Bora, et al., Phys. Chem. Chem. Phys., 2011, 13, 12488–12496.
- 25 J.A. Mikroyannidis, M.M. Stylianakis, P. Suresh, et al., Energy Environ. Sci., 2009, 2, 1293.
- **26** X. Yin, W. Que, and F. Shen, *J. Sol-Gel Sci. Technol.*, 2012, **63**, 279–285.
- 27 Y. Lou, S. Yuan, Y. Zhao, et al., Dalton Trans., 2013, 42, 5330-5337.
- 28 Z.H. Chen, Y.B. Tang, C.P. Liu, et al., J. Phys. Chem. C, 2009, 113, 13433–13437.
- 29 C.K.N. Peh, L. Ke, and G.W. Ho, *Mater. Lett.*, 2010, **64**, 1372–1375.
- **30** T. Bora, H.H. Kyaw, S. Sarkar, *et al.*, *Beilstein J. Nanotechnol.*, 2011, **2**, 681–690.
- 31 V. Dhas, S. Muduli, W. Lee, et al., Appl. Phys. Lett., 2008, 93, 243108.
- 32 M.-Y. Lu, H.-A. Chen, S.-Y. Chen, et al., Honolulu PRIME Meeting, 2012, MA2012-02, 2871.
- 33 A. Pandikumar, K.M. Saranya, and R. Ramaraj, Appl. Phys. Lett., 2012, 101. 10.1063/1.4748287
- **34** F. Al-juaid, A. Merazga, F. Abdel-wahab, and M. *Al-amoudi*, 2012, **2012**, 192–196.
- **35** M. Bokhari, A.K. Kasi, J.K. Kasi, et al., 3M-NANO, International Conference on Manipulation, Manufacturing and Measurement on the Nanoscale, 2013, 4, 243–246.
- **36** M.H. Lai, M.W. Lee, G.J. Wang, and M.F. Tai, *Int. J. Electrochem. Sci.*, 2011, **6**, 2122–2130.
- **37** N. Mir, M. Salavati-Niasari, and F. Davar, *Chem. Eng. J.*, 2012, **181–182**, 779–789.
- 38 B. Kilic, T. Günes, I. Besirli, et al., Appl. Surf. Sci., 2014, 318, 32–36.
- **39** J.B. Baxter and E.S. Aydil, *Sol. Energy Mater. Sol. Cells*, 2006, **90**, 607–622.
- 40 J.B. Baxter, A.M. Walker, K. Van Ommering, and E.S. Aydil, *Nanotechnology*, 2006, 17, S304–S312.